

# UC Santa Cruz

## UC Santa Cruz Previously Published Works

### Title

The Pre-Existing Human Antibody Repertoire to Computationally Optimized Influenza H1 Hemagglutinin Vaccines.

### Permalink

<https://escholarship.org/uc/item/8f92b05j>

### Journal

The Journal of Immunology, 209(1)

### ISSN

0022-1767

### Authors

Nagashima, Kaito  
Dzimianski, John V  
Han, Julianna  
[et al.](#)

### Publication Date

2022-07-01

### DOI

10.4049/jimmunol.2101171

Peer reviewed



# HHS Public Access

Author manuscript

*J Immunol.* Author manuscript; available in PMC 2023 July 01.

Published in final edited form as:

*J Immunol.* 2022 July 01; 209(1): 5–15. doi:10.4049/jimmunol.2101171.

## The pre-existing human antibody repertoire to computationally optimized influenza H1 hemagglutinin vaccines

Kaito Nagashima<sup>1,2</sup>, John V. Dzimianski<sup>3</sup>, Julianna Han<sup>4</sup>, Nada Abbadi<sup>1,2</sup>, Aaron D. Gingerich<sup>2</sup>, Fredejah Royer<sup>2</sup>, Sara O'Rourke<sup>3</sup>, Giuseppe A. Sautto<sup>2</sup>, Ted M. Ross<sup>1,2</sup>, Andrew B. Ward<sup>4</sup>, Rebecca M. DuBois<sup>3</sup>, Jarrod J. Mousa<sup>1,2,5,\*</sup>

<sup>1</sup>Department of Infectious Diseases, College of Veterinary Medicine, University of Georgia, Athens, GA, USA

<sup>2</sup>Center for Vaccines and Immunology, College of Veterinary Medicine, University of Georgia, Athens, GA, USA

<sup>3</sup>Department of Biomolecular Engineering, University of California Santa Cruz, Santa Cruz, CA, USA

<sup>4</sup>Department of Integrative Structural and Computational Biology, The Scripps Research Institute, La Jolla, CA, USA

<sup>5</sup>Department of Biochemistry and Molecular Biology, Franklin College of Arts and Sciences, University of Georgia, Athens, GA, USA

### Abstract

Computationally optimized broadly reactive antigen (COBRA) hemagglutinin (HA) immunogens have previously been generated for several influenza subtypes to improve vaccine-elicited antibody breadth. As nearly all individuals have pre-existing immunity to influenza viruses, influenza-specific memory B cells will likely be recalled upon COBRA HA vaccination. We determined the epitope specificity and repertoire characteristics of pre-existing human B cells to H1 COBRA HA antigens. Cross-reactivity between wild type HA and H1 COBRA HA proteins P1, X6, and Y2 were observed for isolated monoclonal antibodies (mAbs). The mAbs bound five distinct epitopes on the pandemic A/California/04/2009 HA head and stem domains, and the majority of the mAbs had HAI and neutralizing activity against 2009 pandemic H1 strains. Two head-directed mAbs, CA09-26 and CA09-45, had HAI and neutralizing activity against a pre-pandemic H1 strain. One mAb, P1-05, targeted the stem region of H1 HA, but did not compete with a known stem-targeting H1 mAb. We determined that mAb P1-05 recognizes a recently discovered HA epitope, the anchor epitope, and we identified similar mAbs using B cell repertoire sequencing. In addition, the trimerization domain distance from HA was critical to recognition of this epitope by mAb P1-05, suggesting the importance of protein design for vaccine formulations. Overall, these data indicate that seasonally vaccinated individuals possess a population of functional H1 COBRA HA-reactive B cells that target head, central stalk, and anchor epitopes, and demonstrate the importance of structure-based assessment of subunit protein vaccine candidates to ensure accessibility of optimal protein epitopes.

\*Corresponding author: jarrod.mousa@uga.edu.

## Introduction

Influenza viruses are a major cause of morbidity and mortality worldwide each year (1). In particular, influenza A viruses (IAVs) and influenza B viruses cause annual epidemics in humans, and IAVs have caused multiple pandemics over the past century (2). Currently, H1N1 and H3N2 IAVs cause epidemic disease (3, 4). Long-term protection to influenza viruses remains a challenge due to high mutation rates caused by a low-fidelity RNA polymerase, which leads to antigenic drift, as well as reassortment events of HA and NA with avian influenza viruses, which is termed antigenic shift (5). Current seasonal influenza vaccines provide protection against matched circulating viral strains. However, vaccine efficacy varies year to year due to mismatches between circulating strains and vaccine strains, as well as differences in hemagglutinin (HA) protein glycosylation patterns between vaccine and circulating strains (6-8). This variability in vaccine efficacy highlights the importance of developing an improved influenza vaccine, which would elicit an immune response to most circulating influenza A and/or B viruses (9). Current vaccines typically elicit strain-specific antibodies, and only a minority show cross-reactivity to other viral subtypes. The antibody response to influenza virus infection and vaccination focuses predominantly on HA. Within HA-targeting antibodies, those targeting the variable globular head domain dominate the response, whereas those that bind the more conserved stem domain are elicited less frequently (10).

H1N1 IAVs have caused two known pandemics, including the Spanish influenza pandemic of 1918-1919, which caused an estimated 40-50 million deaths, and the 2009 swine influenza pandemic, which caused an estimated 575,000 deaths (11). Circulating 2009 pandemic pH1N1/09-like viruses have replaced pre-2009 seasonal H1N1 influenza viruses in the human population (11). Antigenic sites defined on the H1 subtype HA have been characterized through mutagenesis studies in the presence of neutralizing antibodies (12). These highly variable sites are present on the immunodominant head domain, and include the Sa, Sb, Ca1, Ca2, and Cb sites (12). More recently discovered antibody epitopes include the receptor-binding site (RBS), the lateral patch, and the intratrimeric epitope, which exhibit broader reactivities (9, 13-15).

Computationally optimized broadly reactive antigen (COBRA) HA immunogens aim to elicit a broader antibody response compared to current seasonal vaccines (16, 17). In this approach, multiple-layered consensus building alignments of HA sequences are used to generate an immunogen encompassing multiple epitopes for a single subtype (16). The resulting constellation of consensus epitopes, focused primarily in the antigenic sites of the head domain, represent diverse sequences that elicit broadly reactive antibodies in several animal models, including in mice and ferrets (16, 17). Structural analysis of COBRA HA immunogens has shown that these antigens resemble wild type HA proteins (18). The primary mechanism of COBRA HA-induced antibodies are through hemagglutination inhibition (HAI) and neutralization via HA head domain-binding antibodies (16). In contrast, stem-directed antibodies do not appear to be a major component of COBRA HA vaccine-induced immunity (19, 20). Some H1 subtype-based COBRA HAs have been previously described that incorporate both seasonal (pre-2009) and pandemic-like

(post-2009) influenza virus HA sequences. These include P1, which incorporates human sequences from 1933 to 1957 and 2009 to 2011 as well as swine sequences from 1931 to 1998, and X6, which incorporates human sequences from 1999 to 2012 (21). The Y2 COBRA HA, encompassing sequences from 2014 to 2016, represents the most recent set of H1 subtype viruses that are antigenically similar to the 2009 pandemic H1N1 virus. Importantly, the Y2 COBRA HA has been shown previously to elicit broadly HAI-active antibodies against recent 2018 and 2019 H1N1 pandemic-like viruses in a mouse model, whereas the P1 and X6 COBRA HAs elicit a less broad response against these isolates (22).

An individual's immune history to influenza also plays a major role in the antibody response to vaccination. For example, the idea of original antigenic sin (OAS) describes the dominant nature of the antibody response to the first influenza virus strain compared to exposures to subsequent strains (23). While COBRA HAs have been shown to be efficacious in naïve as well as pre-immune mouse and ferret models of influenza infection, pre-existing immunity to COBRA HAs in humans has not been investigated. This is important to understand as these antigens move toward clinical trials. Here, we identify epitope and repertoire characteristics of the pre-existing antibody response from previous infection and vaccination that is recognized by H1 COBRA HA antigens. We show that human antibodies and B cells that cross-react with COBRA HAs, predominantly with the Y2 COBRA HA and a minority with the P1 and X6 COBRA HAs, are present in individuals vaccinated with the 2017-2018 and 2019-2020 quadrivalent influenza vaccine (QIV). A panel of 26 monoclonal antibodies (mAbs) was isolated, and these mAbs bind five distinct epitopes on the A/California/04/2009 HA protein, including an epitope near the viral membrane, termed the anchor epitope. Moreover, a subset of these antibodies bind both pre- and post-2009 pandemic strains with demonstrable HAI and neutralization activity. Overall, our data identify the major epitopes and repertoire characteristics of pre-existing human antibodies that recognize COBRA HA antigens.

## Materials and Methods

### Human subject samples.

All human studies were approved by the University of Georgia Institutional Review Board. mAb isolation was conducted from subjects aged 22 to 51 years vaccinated with the 2017-2018 seasonal influenza vaccine (Fluzone) from peripheral blood mononuclear cells (PBMCs) isolated from blood draws 21-28 days following vaccination. 80% (4/5) of these subjects showed HAI titers >40 to at least one pre-2009 H1 virus before vaccination. Repertoire sequencing was completed from a single human subject vaccinated with the 2019-2020 influenza vaccine (Fluzone) from blood obtained 28 days following vaccination.

### B cell expansion of human subject PBMCs.

PBMCs were plated at a density of 25,000 cells/well in a 96-well plate on a layer of gamma-irradiated NIH 3T3 cells (20,000 cells/well) expressing hCD40L, hIL-21, and hBAFF in the presence of CpG and cyclosporine A as previously described (24, 25). B cell supernatants were screened by enzyme-linked immunosorbent assay (ELISA) at 7 days post-plating of PBMCs.

### Expression and purification of recombinant influenza HA proteins.

Trimeric wild-type HA or COBRA HA ectodomains were expressed and purified in Expi293F cells following the manufacturer's protocol and as previously described (26). Collected supernatants containing the HA antigens were purified on a HisTrap Excel column following the manufacturer's recommended protocol. Eluted fractions were pooled and purified proteins were verified for integrity by probing with an anti-HIS tag antibody (Biolegend) as well as with subtype-specific mAbs via SDS-PAGE and Western blot.

### ELISA screening of B cells, hybridoma supernatants, mAbs, and rAbs.

Untreated 384-well plates (VWR) were coated with recombinant HA proteins diluted to 2 µg/mL in PBS at 4 °C overnight. Plates were washed once with water, then blocked with 2% blocking buffer (PBS + 2% non-fat dry milk (Bio-Rad) + 2% goat serum + 0.05% Tween-20) for 1 hr at room temperature. Plates were washed three times with water, and 25 µL of B cell supernatants, hybridoma supernatants, mAbs, or recombinant antibodies (rAbs) were added. mAbs and rAbs were serially diluted three-fold in PBS from 20 µg/mL prior to addition for twelve total dilutions. Plates were incubated at 37 °C for 1 hr, then washed three times with water. Goat anti-human IgG Fc-AP secondary antibody (Southern Biotech), diluted 1:4000 in 1% blocking buffer (1:1 dilution of PBS and 2% blocking buffer), was added and plates were incubated at room temperature for 1 hr. Plates were then washed five times with PBS-T (PBS + 0.05% Tween-20). *p*-Nitrophenyl phosphate (PNPP) substrate, diluted in substrate buffer (1.0 M Tris + 0.5 mM MgCl<sub>2</sub>, pH=9.8) to 1 mg/mL, was added, and plates were incubated for 1 hr and read at 405 nm on a BioTek plate reader. To quantify HA-reactive IgG from each subject, plates were coated overnight with eight two-fold serial dilutions of human plasma IgG standard (Athens Biotechnology) starting at 10 µg/mL. All steps were followed as for antigen, except PBS was used in the primary antibody step. GraphPad Prism was used to interpolate antigen-reactive IgGs from the human plasma IgG standard curve. The EC<sub>50</sub> value for each mAb was determined by using the four-parameter logistic curve fitting function in GraphPad Prism software.

### Generation of HA-reactive mAbs.

Eight days following plating of PBMCs, wells identified to contain positive B cells by ELISA were selected for electrofusion to generate hybridomas as previously described (24, 25). Hybridomas were plated in 384-well plates for HAT selection, and grown for 14 days at 37°C, 5% CO<sub>2</sub>. Following screening by ELISA, hybridomas were single-cell sorted using a MoFlo Astrios cell sorter using live/dead staining by propidium iodide. The sorted hybridomas were cultured in 25% Media E (StemCell) + 75% Media A (StemCell) for two weeks, then subjected to another round of screening by ELISA. Hybridomas with the highest signal were grown in 250 mL serum-free media (Gibco) for approximately one month. Secreted mAbs were purified using a Protein G column (GE Healthcare) and concentrated for use in downstream assays.

### Hybridoma sequencing.

Hybridoma cell lines encoding each mAb were sequenced utilizing the primers described by Guthmiller *et al.* (27). Briefly, RNA was extracted from each hybridoma and cDNA was

generated using the SuperScript IV First-Strand cDNA Synthesis Kit (Invitrogen). A nested PCR protocol was used to generate sequencing products. In the first nested PCR step, a primer mix specific to the heavy, kappa, or lambda chain *V* gene and the constant region were used to amplify the variable region using the cDNA as template. In the second PCR step, the first PCR product was used as a template with a nested primer mix to improve product specificity and yield. The second nested PCR products were sequenced using the constant region primer and the *V*, *D*, and *J* alleles were identified by IMGT/V-QUEST (28). Percent identity of mAb variable regions to germline were calculated as the similarity to the germline allele at the nucleotide level using IMGT/V-QUEST (28).

### Hemagglutination inhibition assay.

The HAI titer for each mAb was determined as previously described (20). Influenza viruses were titered to eight HAUs (hemagglutination units). 50  $\mu$ L of mAbs or rAbs diluted to 20  $\mu$ g/mL in PBS were added to the first well of a 96-well U-bottom plate (VWR), and diluted two-fold in PBS for 25  $\mu$ L mAb total per dilution. Eight HAUs of virus were added in a 1:1 ratio to each mAb dilution, and each well was mixed and incubated for 20 min at room temperature. Following this, 50  $\mu$ L of 1.0% turkey red blood cells (Lampire) were added per well. Plates were read 45 min after the addition of 1.0% turkey red blood cells.

### Focal reduction assay.

Focal reduction assays (FRAs) were completed for each mAb as previously described (20). MDCK cells were plated in 96-well plates overnight to achieve >95% confluency the next day. Cells were washed twice with PBS, and 50  $\mu$ L of virus growth media (VGM: DMEM + 2  $\mu$ g/mL TPCK-trypsin + 7.5% BSA) were added and the plates were returned to the incubator at 37°C, 5% CO<sub>2</sub>. mAbs at 20, 8, or 1  $\mu$ g/mL were serially diluted two-fold in VGM, and virus was diluted to a concentration of 1.2x10<sup>4</sup> FFU/mL in VGM. MDCK cells were washed with PBS and 25  $\mu$ L serially diluted mAbs were added, followed by 25  $\mu$ L of 1.2x10<sup>4</sup> FFU/mL of virus. Plates were incubated at 37 °C, 5% CO<sub>2</sub> for 2 hr, and then 100  $\mu$ L/well of overlay media (1.2% Avicel + modified Eagle media (MEM)) were added and incubated overnight. The overlay was removed and wells were washed twice with PBS. Ice-cold fixative (20% formaldehyde + 80% methanol) was added and plates were incubated at 4 °C for 30 min. Plates were washed twice with PBS and permeabilization buffer (PBS + 0.15% glycine + 0.5% Triton-X 100) was added, followed by a 30 min incubation. Plates were washed three times with PBS-T and primary IAV anti-NP mouse antibody (IRR), diluted 1:2000 in ELISA buffer (PBS + 10% goat serum + 0.1% Tween-20), was added. Plates were incubated at room temperature for 1 hr. Plates were then washed three times with PBS-T and secondary goat anti-mouse IgG-HRP antibody (Southern Biotech), diluted 1:4000 in ELISA buffer, was added. Plates were incubated at room temperature for 1 hr and then washed with PBS-T. KPL TrueBlue Peroxidase substrate was added per well and plates were incubated for 10-20 min. Plates were washed, dried, and foci were enumerated using an ImmunoSpot S6 ULTIMATE reader with ImmunoSpot 7.0.28.5 software (Cellular Technology Limited). Neutralizing IC<sub>50</sub>s were calculated using the GraphPad Prism four-parameter logistic curve fitting function.

### Epitope binning by biolayer interferometry.

The panel of mAbs isolated from human subjects were competed for binding using the A/California/04/2009 HA protein on the OctetRED384 system as previously described (24). Anti-penta-HIS biosensors (Sartorius) were immersed in kinetics buffer (PBS + 0.5% BSA + 0.05% Tween-20) for 60 s to obtain a baseline reading. Biosensors were then loaded with 100 µg/mL of A/California/04/2009 HA protein diluted in kinetics buffer for 60 secs. Biosensors were returned to kinetics buffer for a baseline of 60 s. Following this, biosensors were immersed in the first mAb (100 µg/mL in kinetics buffer) for 300 s for the association step. The biosensors were then immersed in the competing, second mAb (100 µg/mL in kinetics buffer) for 300 s. The biosensors were then regenerated in 0.1 M glycine, pH = 2.7 and PBS alternately for three cycles before proceeding to the next mAb competition set. The extent of competition was calculated as the percentage of the signal from the second mAb in the second association step in the presence of the first mAb to that of the second mAb alone in the first association step for all biosensors. A ratio of  $\leq 33\%$  was considered complete competition,  $>33$  and  $\leq 67\%$  moderate competition, and  $>67\%$  no competition.

### Antibody-dependent phagocytic activity of mAbs.

To measure antibody-dependent phagocytic activity,  $2 \times 10^9$  1-µm Neutravidin-coated yellow-green FluoSpheres (Invitrogen #F8776) were resuspended in 1 mL of 0.1% PBS. The FluoSpheres were then centrifuged at 5000 rpm for 15 minutes, 900 µL supernatant was removed, and the FluoSpheres were resuspended with 900 µL of 0.1% PBS. This process was repeated for a second wash, then the FluoSpheres were resuspended with 20 µg of biotinylated Y2 protein. The FluoSpheres were then incubated overnight at 4 °C, protected from light, with end-to-end rocking. Next, HA-specific antibodies were diluted in complete RPMI media (cRPMI, RPMI + 10% FBS) to a final concentration of 1 µg/mL in a U-bottom 96-well plate. Then, 20 µL of antibody dilution was transferred into a clean F-bottom 96-well plate, and 10 µL of FluoSpheres were added with the antibody followed by a 2 hr incubation at 37 °C for opsonization. After 1.5 hr, THP-1 cells were centrifuged at  $200 \times g$  for 5 min, washed once with PBS, then resuspended in culture medium (RPMI & 10% FBS) at a concentration of  $5 \times 10^5$  cells/mL. Then, 200 µL of cells were added to each well and incubated at 37 °C with 5% CO<sub>2</sub> while shaking for 6 hr. Once the incubation finished, the plate was then centrifuged at 2000 rpm for 5 min. Then, 100 µL was pipetted out of each well and replaced with 100 µL of cold 4% paraformaldehyde to fix the cells. The plate was then left at room temperature for 20 min, protected from light. The plate was then stored at 4 °C in the dark. Cells were then analyzed with a NovoCyte Quanteon flow cytometer.

### Expression and purification of recombinant proteins for electron microscopy.

For EM studies, Y2 HA COBRA was cloned using Gibson assembly into a derivative of pcDNA3.1+ (29). Plasmids for the P1-05 heavy and light chain were synthesized (Genscript) and cloned into pcDNA3.1+. Cells and media were purchased from Thermo Fisher Life Technologies unless stated otherwise. Y2 HA protein expression was initiated by transfection of endotoxin free DNA into CHO-S cells using flow electroporation technology (MaxCyte). Transfected cells were suspended in CD OptiCHO supplemented with 2 mM GlutaMAX, HT, 0.1% pluronic acid, and incubated at 37 °C, 8% CO<sub>2</sub>, 85% humidity in



an orbital shaker (Kuhner). After 24 hrs, cultures were supplemented with 1 mM sodium butyrate, and the culture temperature was dropped to 32°C. Cultures were supplemented daily with MaxCyte CHO A Feed (0.5% yeastolate, 2.5% CHO-CD Efficient Feed A, 2 g/L glucose, 0.25 mM GlutaMAX). The media was harvested 8-12 days post-transfection and filtered. For purification of Y2, media was diluted with an equal volume of Buffer A (500 mM NaCl, 20 mM sodium NaH<sub>2</sub>PO<sub>4</sub>, 20 mM imidazole) and loaded onto a 1 mL HisTrap column (GE Healthcare). The column was washed with Buffer A and the protein eluted with a gradient to Buffer B (500 mM NaCl, 20 mM NaH<sub>2</sub>PO<sub>4</sub>, 500 mM imidazole) on an ÄKTA Pure chromatography system (GE Healthcare). Fractions containing the protein were pooled, concentrated, and further purified and buffer exchanged on a Superdex 200 10/300 column (GE Healthcare) equilibrated in PBS (Sigma). Fractions were pooled and concentrated, then flash frozen in liquid N<sub>2</sub> and stored at -80°C until use. For P1-05, the mAb was purified using a 1 mL HiTrap Protein A HP column (GE Healthcare). The media was diluted with an equal volume of Protein A IgG Binding Buffer (Thermo Scientific) and loaded onto the column. The column was washed with binding buffer, then eluted with a gradient to Protein A IgG Elution Buffer (Thermo Scientific). To adjust the pH, 55 µl of 1.89 M Tris pH 8 was added per 1 mL fraction. Fab was generated and purified using the Pierce™ Fab Preparation Kit according to the manufacturer's instructions (Thermo Scientific). The Fab product in PBS was flash frozen in liquid N<sub>2</sub> and stored at -80 °C until use.

#### **Cloning and expression of Y2 COBRA with a thrombin cleavage site.**

Y2 COBRA was cloned into the pBacPAK8 vector in frame with an N-terminal gp67 signal sequence and C-terminal thrombin cleavage site, T4 fibrin domain, and hexahistidine/StrepTag II tags. The construct design results in predicted vector supplied sequences of AATNA and LVPRGSPGSGYIPEAPRDGQAYVRKDGWVLLSTFLGHHHHHHGGSWHPQFEK at the N- and C-termini, respectively. Baculovirus was generated using the *flashBac*™ kit according to the manufacturer's instructions (Mirus Bio). The protein was expressed in 2 L of Sf9 cells at 2×10<sup>6</sup> cells/mL maintained in ESF921 media (Expression Systems) by adding 25 mL virus per liter of culture. The media was harvested after 3 days, pH adjusted with NaCl and Tris pH 8, and stored at -20°C. Prior to purification, the thawed media was filtered and concentrated to 150-200 mL by tangential flow with a Vivaflow® 200 (Sartorius). The resulting sample was diluted with an equal volume of Buffer A, filtered, and loaded onto a 5 mL HisTrap column (GE Healthcare). The column was washed with Buffer A and the protein eluted with a gradient to Buffer B. The protein was pooled, concentrated, and supplemented with 5% glycerol prior to flash freezing and storage at -80 °C.

#### **Kinetic assays by biolayer interferometry.**

Biolayer interferometry kinetic assays were performed in triplicate on the Octet® Red384 system (Sartorius) with a buffer containing PBS, 1% BSA, and 0.05% Tween. Anti-penta-HIS biosensors were immersed in buffer for 120 s, then loaded with 10 µg/mL Y2 for 300 s. The biosensors were then dipped into buffer for 120 s to obtain a baseline, dipped into buffer containing P1-05 Fab in a dilution series ranging from 54 nM to 0.67 nM for 300 s, and buffer for 600 s to measure dissociation. The data were processed in the Octet Data Analysis HT software v7 (Sartorius). Each curve was reference subtracted, aligned



to the baseline, and aligned for inter-step correction through the dissociation step for each curve. Each replicate was fit globally for well-resolved curves in the dilution series using a 1:1 binding model. Parameters were optimized based on the  $R^2$ ,  $\chi^2$ , and individual  $K_D$  error values to maximize the goodness of fit. The final reported  $K_D$  value ( $98.5 \pm 32.3$  pM) represents the mean  $\pm$  standard deviation of three independent experiments.

### **Electron microscopy of the Y2+P1-05 complex.**

The protein samples were thawed on ice. To generate the immune complex, P1-05 Fab and Y2 COBRA produced in CHO cells were combined in a 3:1 Fab:HA trimer ratio and incubated at room temperature for 1 hr. For negative stain analysis, the immune complex was deposited at 15  $\mu\text{g}/\text{mL}$  onto carbon-coated, glow-discharged, 400 mesh copper grids (EMS) and stained with 2% w/v uranyl formate. The sample was imaged on an Arctica Talos 200C electron microscope (FEI) operating at 73,000x nominal magnification with a Falcon II direct electron detector and a CETA 4k camera (FEI). Micrographs were collected with Legion and particles were picked using a difference of Gaussians particle picker and processed with Appion (30-32). Particles were classified in 2D and 3D in Relion 3.0 and Cryosparc2 and reconstructed in 3D in Cryosparc2 (33, 34). Figures were made in UCSF Chimera (35).

### **Single-cell V(D)J sequencing and analysis.**

PBMCs were stained with the following antibodies and proteins for flow sorting: anti-CD19-APC (1:10 dilution, clone HIB19, cat. no. 982406, BioLegend), anti-IgD-FITC (1:20 dilution, clone IA6-2, cat. no. 348206, BioLegend), anti-IgM-FITC (1:20 dilution, clone MHM-88, cat. no. 314506, BioLegend), Ghost Dye Red (1:1000), Y2-PE (1:20 dilution), and Y2-BV605 (1:20). AviTagged Y2 COBRA HA proteins containing the Y98F mutation to reduce sialic acid binding were biotinylated using the BirA biotin-protein ligase in the BirA500 kit (Avidity) and complexed to streptavidin-fluorophores SA-PE (1:500 dilution, cat. no. S866, Thermo Fisher) and SA-BV605 (1:250 dilution, cat. no. 405229, BioLegend). CD19<sup>+</sup>IgM/IgD<sup>-</sup>PE<sup>+</sup>BV605<sup>+</sup> double-positive, antigen-specific B cells were flow sorted on the MoFlo Astrios and resuspended in PBS+0.04% BSA. These cells were then used to generate Single Cell 5' v2 Dual Index V(D)J libraries using the 10X Chromium Next GEM Single Cell 5' Reagent Kit v2 (10X Genomics). Libraries were then sequenced using a NextSeq 550 sequencer (Illumina). Single-cell V(D)J FASTQ files were generated and demultiplexed using Cell Ranger v4.0.0 and data were visualized using the Loupe VDJ v3.0.0 browser. Only B cells with complete, ungapped variable regions and singly paired heavy and light chains were considered for downstream analysis. Six B cell receptor sequences were expressed as recombinant IgGs in 293 cells and used for ELISAs and HAIs.

## **Results**

### **COBRA HA-specific B cell responses**

To determine the size of the H1 COBRA HA-reactive B cell population within seasonally vaccinated individuals, total B cells from four vaccinated subjects (2017-2018 cohort) were stimulated on an irradiated feeder layer as previously described (24). B cell supernatants were assayed for activity against A/California/04/2009 HA, P1 COBRA HA, and X6

COBRA HA recombinant proteins by ELISA. As expected, HA- and COBRA HA-reactive IgG titers were higher in day 21 post-vaccination samples compared to those obtained pre-vaccination (Figure 1). Comparisons of A/California/04/2009 HA-reactive IgG titers to those of P1 HA- and X6 HA-reactive IgGs indicated that binding to A/California/04/2009 HA protein was consistently higher. The majority of subjects demonstrated significant P1 HA-reactive IgG titers that, while lower than A/California/04/2009 HA-reactive IgG titers, were higher than or equivalent to X6 HA-reactive IgG titers in three of four subjects. The disparity in antibody titers between wild-type A/California/04/2009 HA- and COBRA HA-reactive proteins may be attributed to the relatively high abundance of pandemic strain-specific antibodies, and the absence of these potential binding epitopes on the P1 and X6 H1 COBRA HA proteins. Moreover, the degree of similarity of each COBRA HA to the A/California/04/2009 HA appeared to be reflected in the degree to which reactive IgG titers were elicited. Namely, the P1 COBRA HA, representing pandemic-like human and swine H1 HA sequences, demonstrates 84.63% identity to A/California/04/2009 HA, whereas the X6 HA, representing seasonal-like H1 HA sequences, demonstrated a lower 80.53% identity to A/California/04/2009 HA.

### Lineage analysis of pre-existing COBRA HA-specific mAbs

To further probe the pre-existing B cell response to COBRA HA antigens, we isolated 26 mAbs from five additional human subjects vaccinated with the 2017-2018 quadrivalent influenza vaccine within the same cohort, using A/California/04/2009 HA and P1 COBRA HA as screening antigens. The antibody-encoding genes were sequenced, and the results indicated the usage of several different immunoglobulin *V* genes across the entire panel (Figure 2, Table S1). When comparing usage of heavy chain genes,  $V_{H1}$ ,  $V_{H3}$ ,  $V_{H4}$ , and  $V_{H5}$  gene families were represented (Figure 2A). Approximately 50% of all mAbs utilized a gene from the  $V_{H3}$  family, and approximately another 50% utilized a gene from the  $V_{H4}$  family. In the light chain, for those mAbs utilizing the kappa chain, many utilized genes  $V_{K3-11}$  and  $V_{K3-15}$ . The remainder used *V* genes  $V_{K3-20}$  or those from  $V_{K1}$  or  $V_{K2}$  families. mAbs utilizing the lambda chain used predominantly  $V_{L3-21}$  and  $V_{L2-14}$ . Paired heavy and light chain *V* genes showed variation across the antibody panel, with the  $V_{H3-7}$ :  $V_{K3-15}$  and  $V_{H4-39}$ :  $V_{L2-14}$  pairings being the most abundant for kappa- and lambda chain-utilizing mAbs, respectively (Figure 2B). The CDR3 regions ranged in length from 10-22 amino acids for the heavy chain, 8-10 amino acids for the kappa chain, and 10-12 amino acids for the lambda chain (Figure 2C). The percent identities of the variable genes to the germline sequence had averages of 93% for both the heavy and kappa chains, and 96% for the lambda chain at the nucleotide level (Figure 2C).

### Binding analysis of COBRA HA-specific human mAbs

P1 and X6 COBRA HA proteins incorporate historical epitopes from both pre- and post-2009 viruses, while Y2 COBRA HA incorporates more recent 2009 pandemic-like sequences from 2014 to 2016, representing the HA epitopes from more recent H1 isolates (22) (Figure 3). The majority of isolated mAbs demonstrated high binding to A/California/04/2009 HA protein by ELISA, with an average  $EC_{50}$  of 30 ng/mL (Figure 4A, Figure S1A). Of these A/California/04/2009 HA protein-reactive mAbs, only a subset demonstrated binding to the divergent P1 and X6 COBRA HA proteins. mAbs P1-02,

P1-05, and 163-20 showed reactivity against the P1 COBRA protein, and mAbs CA09-26, CA09-30, CA09-45, P1-02, and P1-05 demonstrated binding to the X6 COBRA protein. The limited mAb binding to P1 and X6 COBRA proteins correlated with the lower reactive B cell frequencies to these respective HAs in Figure 1. All mAbs had similar EC<sub>50</sub> values and reactivities to the Y2 COBRA HA compared to A/California/04/2009 HA (Figure 4A, Figure S1A). No binding was observed for any mAb to the H3 subtype HA HK14 or to an irrelevant antigen control (Figure S1A). We also determined whether mAbs were broadly reactive by utilizing a chimeric HA protein bearing a H6 HA head and a H1 HA stem (cH6/1) (Figure 4A). mAb P1-05 bound to the chimeric protein with high avidity, suggesting this mAb may bind the stem region of the H1 HA protein, or some other conserved epitope present in both H1 and H6 HAs. These results indicate that 2017-2018 QIV-vaccinated subjects possessed mAbs with potent binding to the 2009 pandemic-like Y2 COBRA HA protein. Moreover, mAbs from different subjects with reactivity against the divergent P1 and/or X6 COBRA HAs were found, although these represented a small part of the total antibody response. Based on these data and the B cell screening data, COBRA HA-reactive B cells constitute part of the human B cell response to influenza vaccination, and COBRA HA antigens can likely recall such B cells targeting both the head and stem regions.

### Functional analysis of COBRA HA-specific mAbs

To characterize the functional activities of the isolated mAbs, HAI and neutralizing activities were assessed (Figure 4B, 4C, S2). The majority of mAbs showed HAI activity against the pandemic-like A/Michigan/45/2015 virus (Figure 4B). These data are consistent with the fact that most mAbs bound the head domain of A/California/04/2009 HA (Figure 4A). Of those mAbs with the highest HAI activity of the panel against the recent pandemic-like A/Michigan/45/2015 virus, CA09-26 and CA09-45 were tested for HAI against two pre-pandemic H1 viruses as these mAbs bind the X6 HA COBRA, which incorporates pre-pandemic sequences, and both target the HA head domain. CA09-26 had HAI activity against A/New Caledonia/20/1999 and A/Brisbane/59/2007 viruses, while CA09-45 had HAI activity against A/New Caledonia/20/1999, and no activity against A/Brisbane/59/2007 (Figure 4B). We next assessed neutralizing activity against A/California/07/2009 (Figure 4C, S2). Approximately 60% of mAbs (16/26 mAbs) neutralized the pandemic A/California/07/2009 virus (A/CA/09). Notably, mAbs CA09-26 and CA09-45 were among the most potent mAbs in the panel with half-maximal inhibitory concentrations (IC<sub>50</sub>s) of 0.013 µg/mL and 0.032 µg/mL, respectively. These two mAbs were also tested for neutralizing activity against A/New Caledonia/20/1999 and A/Brisbane/59/2007 (Figure 4C). They had IC<sub>50</sub> values of 0.081 µg/mL and 0.286 µg/mL, respectively, against A/New Caledonia/20/1999, indicating potent neutralization activity (Figure S2). However, these two mAbs did not demonstrate neutralizing activity against the A/Brisbane/59/2007 virus, in accordance with the observation that little to no HAI activity was observed for the same strain.

Neutralization-independent, Fc-dependent activities are an important aspect of anti-influenza antibodies that bind both the head and stem domains (36-38). Stem-binding antibodies elicited by P1 HA vaccination also demonstrate Fc activity by inducing cellular cytotoxicity (20). To determine the extent of one such Fc effector function, antibody-dependent

phagocytosis (ADP) activity was measured by assessing the capacity for the monocytic THP-1 cell line to phagocytose Y2 COBRA HA-coated beads through mAb binding (Figure 4D, S3A, S3B). The entire mAb panel demonstrated ADP activity relative to a negative mAb control. These included both neutralization/HAI-positive mAbs as well as mAbs that did not demonstrate significant HAI or neutralization activity.

### Multiple distinct epitopes on the A/California/04/2009 HA are bound by isolated mAbs.

To determine the epitopes bound by the panel of 26 mAbs isolated from these vaccinated subjects, biolayer interferometry-based epitope binning was performed as previously described (24, 39). Biosensors were loaded with A/California/04/2009 HA, associated with one mAb, and then exposed to a second mAb to determine mAb competition (Figure 5). Control mAbs Ab6649, 5J8, and CR6261 were utilized to determine the relative locations of each epitope. Ab6649 binds the lateral patch, proximal to the Sa antigenic site; 5J8 binds the receptor-binding site (RBS), comprising antigenic sites Sb and Ca2; CR6261 binds a conserved portion of the stem region found for all group 1 viruses (Figure 5A). Five distinct epitopes on A/California/04/2009 HA protein were distinguished (Figure 5B). Of the epitopes on the globular head domain, two known major epitopes, termed epitope 1 and epitope 3, corresponding to those of mAbs Ab6649 and 5J8, respectively, were identified. MAbs competing with Ab6649 were comprised in part of those using the heavy chain gene  $V_{H3-23}$ , including mAbs CA09-19 and CA09-29, similar to those described recently that bind the lateral patch, although these mAbs did not contain the characteristic YXR motif within the heavy chain CDR3 (40). The position of one predominantly bound epitope, epitope 2, could not be identified by epitope binning with the control mAbs used. Two other epitopes, characterized only by the competition of a single mAb to itself, were epitopes 4 and 5, which correspond to mAbs CA09-38 and P1-05, respectively. No mAbs competed with CR6261, indicating that although mAb P1-05 may target the stem, as evidenced by binding to the cH6/1 protein (Figure 3, S1A), this mAb might target a different epitope on the stem of the H1 HA protein. Overall, these data suggest that the epitopes bound by mAbs from vaccinated subjects are likely comprised, in part, of regions within or around conserved sites on the head domain, such as those involving the RBS and the lateral patch, in addition to portions of the stem.

Epitope 5, characterized by binding by mAb P1-05, was likely located on the stem of the H1 HA protein yet did not overlap with other antibody epitopes (Figure 5). To determine the epitope of mAb P1-05, we generated a complex of Y2 HA bound to P1-05 Fab fragments and evaluated its structure by negative-stain electron microscopy (EM) (Figure 6A, 6B). The 2D class averages revealed that P1-05 binds to the base of the HA stem in an upward angle (Figure 6B). We also observed that insertion of residues between the Y2 C-terminus and the Foldon trimerization domain disrupted mAb P1-05 binding, potentially due to trimer splaying and disruption of this membrane proximal epitope (Figure 6C). Recently, a similar class of mAbs targeting this region on HA, termed the “anchor” epitope, was discovered, and such mAbs protect against H1N1 infection in mice (41, 42). Anchor mAbs do not compete with known stem mAbs and utilize  $V_{K3-11}$  or  $V_{K3-15}$  kappa V genes that encode a germline encoded NWP motif in the CDR3 region (42). The restricted light chains can pair with  $V_{H3-23}$ ,  $V_{H3-30}/V_{H3-30-3}$ , or  $V_{H3-48}$  V genes. mAb P1-05 utilizes  $V_{K3-11}$  paired

with  $V_H3-23$  and also possesses the NWP motif. Furthermore, it was also recently reported that binding of anchor mAbs is disrupted by the use of a GCN4 trimerization domain (42), which has different spacing than the Foldon domain, which matches our data with the disruption of binding observed in Figure 6C. These data affirmed that P1-05 binds to the anchor epitope in the stem, consistent with data from Figure 3A, rather than another conserved HA epitope in the head domain. These observations are critical for subunit HA protein vaccine development as they indicate the importance of antigen design, stability, and the incorporation of mAb binding avidity studies to ensure that important epitopes are properly displayed on candidate vaccine antigens.

### Repertoire analysis of Y2-specific B cells

To further probe the repertoire of pre-existing COBRA HA-specific B cells in a more recent vaccine season, we conducted a single-cell RNA sequencing experiment using B cells from a single subject vaccinated with the 2019-2020 seasonal influenza vaccine. Approximately 3000  $CD19^+IgM^-IgD^-$  B cells positive for the Y2 COBRA HA were sorted and subjected to 10X barcoding (Figure 7, S3C). Prior to loading onto the 10X controller, sorted Y2-specific cells were supplemented with the CA09-26 hybridoma clone as a loading control. 119 unique paired heavy and light chains were obtained following data demultiplexing and analysis compared to the human genome database. Similar to the mAb sequencing, the  $V_H1$  and  $V_H4$  gene families were highly prevalent in the B cell repertoire. In particular,  $V_H4-39$  and  $V_H4-59$  were prevalent in both mAb sequencing and B cell sequencing results. We also identified several additional mAbs utilizing the  $V_H3-23$  gene, with one in particular (clone 70) having an NWP motif in a paired  $V_K3-15$  light chain, although this clone utilized a  $J_K2$  gene, rather than the  $J_K4$  or  $J_K5$  gene, which were previously used to identify anchor epitope-specific mAbs (42) (Table S1). A fraction of clones using the  $V_H1-69$  gene were also identified, which is utilized by mAbs targeting the stalk epitope. Hence, pre-existing mAbs binding Y2 utilize a relatively diverse repertoire.

To identify whether these B cell clones were reactive against the baiting Y2 antigen, we recombinantly expressed six selected clones, 32, 58, 60, 70, 73, and 86, as recombinant antibodies (rAbs). We then evaluated binding to the Y2 and cH6/1 HAs, as well as HAI activity against the more recent 2019 H1N1 strain A/Guandong-Maonan-SWL-1536/2019 (A/GM/19) (Figure 7E, 7F, S1B). All rAbs bound the Y2 COBRA HA with high affinity (Figure 7E) but had no significant activity against the H1 HA stem as assessed by cH6/1 HA binding, including clone 70, which possessed the NWP motif but used the  $J_K2$  gene. To evaluate functionality, we performed HAI assays against the recent A/GM/19 virus. All but one rAb, 70, possessed HAI activity against this strain (Figure 7F). These data suggest that Y2-reactive antibodies isolated from PBMCs from a 2019-2020 seasonally vaccinated subject generally possess functionality against recent 2009 pandemic-like H1N1 strains, including a drifted 2019 virus. Importantly, this virus represents a strain not included in the original design period of the Y2 COBRA HA (2014-2016), yet rAbs derived from Y2-reactive B cells possessed HAI activity, indicating functionality against a future H1N1 strain with the COBRA HA platform.



## Discussion

H1 COBRA HA antigens have been successful at broadening the antibody response compared to wild-type HA sequences in naïve and pre-immune mouse and ferret models of influenza infection (21, 22). However, pre-existing immunity to influenza in humans remains a major challenge to overcome due to repeated previous exposure to the influenza HA protein during infection and vaccination events. In this study, we sought to determine the extent of the H1 subtype COBRA HA-reactive pre-existing B cell repertoire in human subjects to predict recall responses as COBRA HA antigens move toward clinical trials. At the oligoclonal B cell level, pre-existing B cell responses were observed for P1 and X6 COBRA antigens in individuals vaccinated with the 2017-2018 seasonal influenza vaccine, which incorporated the pandemic-like A/Michigan/45/2015 vaccine strain. COBRA HA-reactive B cell responses were lower than those observed for A/California/04/2009 HA protein, likely due to the loss of strain-specific variable head epitopes and incorporation of seasonal pre-pandemic and swine HA sequences in the X6 and P1 antigens, respectively. While it is likely that seasonal vaccination induced these COBRA HA-reactive B cells, it is possible that prior exposures to H1 viruses before vaccination may also have induced these HA-reactive B cell subsets. Moreover, we examined antibody responses to COBRA HAs in a small cohort of five vaccinated subjects, which may limit our conclusions on the extent of pre-existing antibodies to H1 COBRA HAs in the general population. Only a small subset of mAbs isolated against A/California/04/2009 HA reacted with P1 and X6 COBRA antigens. In contrast, the mAb binding profile to the recently described Y2 COBRA HA, which incorporates more recent 2009 pandemic-like H1 sequences from 2014-2016, was similar to that observed for the A/California/04/2009 HA protein. The presence of such Y2-reactive mAbs may indicate specificities against common epitopes present only in more recent 2009 pandemic-like strains but not in historical pre-2009 viruses, which could be more relevant for immunity against future H1 virus exposures. The majority of the mAbs had HAI activity and neutralizing activity against A/Michigan/45/2015 and A/California/07/2009, and two head-binding mAbs that bind the X6 protein, CA09-26 and CA09-45, had HAI activity and neutralizing activity against the pre-pandemic strain A/New Caledonia/20/1999. These data suggest that X6 HA-reactive mAbs are mainly endowed with functional activity against both pre-pandemic and pandemic-like H1 viruses. Overall, the amino acid similarity of COBRA HA antigens to A/California/04/2009 HA correlated with high B cell and mAb reactivity. In addition to binding, neutralization, and HAI activity, we also assessed if COBRA HA-reactive mAbs had Fc-mediated functions, namely ADP, and all mAbs were able to induce THP-1 phagocytosis of Y2-coated beads.

Several epitopes on the H1 HA protein have been previously defined (9), and we determined mAb epitopes on the A/California/04/2009 HA protein using biolayer interferometry. The majority of the mAbs targeted three head-binding epitopes on the Sa and Sb/Ca2 sites, and an undefined epitope, epitope 2, which is currently under structural characterization. One limitation of the BLI-based binning assay is that it does not definitively characterize antibody breadth and functionality, only providing data on the relative positions of epitopes. For instance, we observed a significant number of mAbs competing with the widely reactive 5J8 and Ab6649 antibodies, yet most isolated mAbs competing with 5J8 and Ab6649 did



not bind as widely, with most lacking reactivity to the divergent P1 and X6 COBRA HAs. mAb CA09-38 did not exhibit HAI or neutralizing activity, nor did it bind the cH6/1 HA, suggesting that this mAb may target an undefined, non-neutralizing epitope on the head. We discovered that P1-05 targets a unique epitope on the H1 HA stem region, and this epitope is similar to the recently described anchor epitope (42). Based on these data, while COBRA antigens were primarily designed to induce broadly reactive antibodies to the head domain, these antigens will likely also recall broadly reactive anchor mAbs in humans in addition to head-based recall and *de novo* antibody responses. Further repertoire analysis in a subject vaccinated with the 2019-2020 seasonal influenza vaccine identified similar sequences to our mAbs targeting the head domain from the 2017-2018 season which possessed HAI activity against a drifted 2019 H1N1 virus, A/Guangdong-Maonan/SWL-1536/2019, indicating that the COBRA-reactive B cell population may be similar across subjects and influenza vaccine seasons.

These data provide evidence that a pre-immune population with exposure to the seasonal influenza virus vaccine exhibits B cell reactivity towards conserved epitopes present on COBRA HA antigens. As the COBRA HA platform enters clinical trials, it is likely that head-specific and some stem-specific antibodies will be elicited as part of a recall response. Moreover, the antibody epitopes identified in this work overlap in part with those previously identified on the head domain near the RBS and the lateral patch, in addition to those on the stem. These epitopes are the focus of future structural studies, particularly for those mAbs that cross-react with the X6 COBRA HA as well as with the HA stem domain. Our data also exemplify the importance of structural analysis of protein epitopes to ensure epitopes that elicit broadly neutralizing antibodies, such as the anchor epitope, remain intact following design optimization for subunit HA vaccines.

## Supplementary Material

Refer to Web version on PubMed Central for supplementary material.

## Funding statement

This work was supported by the Collaborative Influenza Vaccine Innovation Centers (CIVIC) contract by the National Institute of Allergy and Infectious Diseases, a component of the NIH, Department of Health and Human Services, under contracts 75N93019C00052 (G.A.S., T.M.R., R.M.D., J.J.M.) and 75N93019C00051 (A.B.W.). J.J.M. is partially supported by National Institutes of Health grant K01OD026569. F.R. was supported by National Institutes of Health NIGMS grant GM109435. T.M.R. is supported as an Eminent Scholar by the Georgia Research Alliance.

## Data availability

The 3D reconstruction of Y2 + P1-05 was deposited to the Electron Microscopy Data Bank under deposition ID EMD-26586: <https://www.ebi.ac.uk/emdb/EMD-26586>.

## References

1. Iuliano AD, Roguski KM, Chang HH, Muscatello DJ, Palekar R, Tempia S, Cohen C, Gran JM, Schanzer D, Cowling BJ, Wu P, Kyncl J, Ang LW, Park M, Redlberger-Fritz M, Yu H, Espenhain L, Krishnan A, Emukule G, van Asten L, Pereira da Silva S, Aungkulanon S, Buchholz U, Widdowson M-A, Bresee JS, Azziz-Baumgartner E, Cheng P-Y, Dawood F, Foppa I, Olsen S, Haber M, Jeffers

- C, MacIntyre CR, Newall AT, Wood JG, Kundi M, Popow-Kraupp T, Ahmed M, Rahman M, Marinho F, Sotomayor Proschle CV, Vergara Mallegas N, Luzhao F, Sa L, Barbosa-Ramírez J, Sanchez DM, Gomez LA, Vargas XB, Herrera aBetsy Acosta, Llanés MJ, Fischer TK, Krause TG, Mølbak K, Nielsen J, Trebbien R, Bruno A, Ojeda J, Ramos H, an der Heiden M, del Carmen Castillo Signor L, Serrano CE, Bhardwaj R, Chadha M, Narayan V, Kosen S, Bromberg M, Glatman-Freedman A, Kaufman Z, Arima Y, Oishi K, Chaves S, Nyawanda B, Al-Jarallah RA, Kuri-Morales PA, Matus CR, Corona MEJ, Burmaa A, Darmaa O, Obtel M, Cherkaoui I, van den Wijngaard CC, van der Hoek W, Baker M, Bandaranayake D, Bissielo A, Huang S, Lopez L, Newbern C, Flem E, Grøneng GM, Hauge S, de Cosío FG, de Moltó Y, Castillo LM, Cabello MA, von Horoch M, Medina Osis J, Machado A, Nunes B, Rodrigues AP, Rodrigues E, Calomfirescu C, Lupulescu E, Popescu R, Popovici O, Bogdanovic D, Kostic M, Lazarevic K, Milosevic Z, Todorovic B, Chen M, Cutter J, Lee V, Lin R, Ma S, Cohen AL, Treurnicht F, Kim WJ, Delgado-Sanz C, de mateo Ontañón S, Larrauri A, León IL, Vallejo F, Born R, Junker C, Koch D, Chuang J-H, Huang W-T, Kuo H-W, Tsai Y-C, Bundhamcharoen K, Chittaganpitch M, Green HK, Pebody R, Goñi N, Chiparelli H, Brammer L, and Mustaqim D. 2018. Estimates of global seasonal influenza-associated respiratory mortality: a modelling study. *Lancet* 391: 1285–1300. [PubMed: 29248255]
2. Flerlage T, Boyd DF, Meliopoulos V, Thomas PG, and Schultz-Cherry S. 2021. Influenza virus and SARS-CoV-2: pathogenesis and host responses in the respiratory tract. *Nat. Rev. Microbiol* 19: 425–441. [PubMed: 33824495]
  3. Jester BJ, Uyeki TM, and Jernigan DB. 2020. Fifty Years of Influenza A(H3N2) Following the Pandemic of 1968. *Am. J. Public Health* 110: 669–676. [PubMed: 32267748]
  4. LaRussa P 2011. Pandemic novel 2009 H1N1 influenza: what have we learned? *Semin. Respir. Crit. Care Med* 32: 393–399. [PubMed: 21858744]
  5. Webster RG, and Govorkova EA. 2014. Continuing challenges in influenza. *Ann. N. Y. Acad. Sci* 1323: 115–139. [PubMed: 24891213]
  6. Soema PC, Kompier R, Amorij JP, and Kersten GFA. 2015. Current and next generation influenza vaccines: Formulation and production strategies. *Eur. J. Pharm. Biopharm* 94: 251–263. [PubMed: 26047796]
  7. Zost SJ, Parkhouse K, Gumina ME, Kim K, Perez SD, Wilson PC, Treanor JJ, Sant AJ, Cobey S, and Hensley SE. 2017. Contemporary H3N2 influenza viruses have a glycosylation site that alters binding of antibodies elicited by egg-adapted vaccine strains. *Proc. Natl. Acad. Sci. U. S. A* 114: 12578–12583. [PubMed: 29109276]
  8. Chang D, and Zaia J. 2019. Why glycosylation matters in building a better flu vaccine. *Mol. Cell. Proteomics* 18: 2348–2358. [PubMed: 31604803]
  9. Nagashima KA, and Mousa JJ. 2021. Next-Generation Influenza HA Immunogens and Adjuvants in Pursuit of a Broadly Protective Vaccine. *Viruses* 13.
  10. Zost SJ, Wu NC, Hensley SE, and Wilson IA. 2019. Immunodominance and Antigenic Variation of Influenza Virus Hemagglutinin: Implications for Design of Universal Vaccine Immunogens. *J. Infect. Dis* 219: S38–S45. [PubMed: 30535315]
  11. Saunders-Hastings PR, and Krewski D. 2016. Reviewing the History of Pandemic Influenza: Understanding Patterns of Emergence and Transmission. *Pathog. (Basel, Switzerland)* 5: 66.
  12. Caton AJ, Brownlee GG, Yewdell JW, and Gerhard W. 1982. The antigenic structure of the influenza virus A/PR/8/34 hemagglutinin (H1 subtype). *Cell* 31: 417–427. [PubMed: 6186384]
  13. Krause JC, Tsibane T, Tumpey TM, Huffman CJ, Basler CF, and Crowe JE. 2011. A Broadly Neutralizing Human Monoclonal Antibody That Recognizes a Conserved, Novel Epitope on the Globular Head of the Influenza H1N1 Virus Hemagglutinin. *J. Virol* 85: 10905–10908. [PubMed: 21849447]
  14. Raymond DD, Bajic G, Ferdman J, Suphaphiphat P, Settembre EC, Moody MA, Schmidt AG, and Harrison SC. 2018. Conserved epitope on influenza-virus hemagglutinin head defined by a vaccine-induced antibody. *Proc. Natl. Acad. Sci. U. S. A* 115: 168–173. [PubMed: 29255041]
  15. Watanabe A, McCarthy KR, Kuraoka M, Schmidt AG, Adachi Y, Onodera T, Tonouchi K, Caradonna TM, Bajic G, Song S, McGee CE, Sempowski GD, Feng F, Urick P, Kepler TB, Takahashi Y, Harrison SC, and Kelsoe G. 2019. Antibodies to a Conserved Influenza Head

- Interface Epitope Protect by an IgG Subtype-Dependent Mechanism. *Cell* 177: 1124–1135.e16. [PubMed: 31100267]
16. Allen JD, Ray S, and Ross TM. 2018. Split inactivated COBRA vaccine elicits protective antibodies against H1N1 and H3N2 influenza viruses. *PLoS One* 13: 1–15.
  17. Darricarrère N, Pougatcheva S, Duan X, Rudicell RS, Chou T, DiNapoli J, Ross TM, Alefantis T, Vogel TU, Kleanthous H, Wei C-J, and Nabel GJ. 2018. Development of a Pan-H1 Influenza Vaccine. *J. Virol* 92: 1–14.
  18. Bar-Peled Y, Huang J, Nuñez IA, Pierce SR, Ecker JW, Ross TM, and Mousa JJ. 2019. Structural and antigenic characterization of a computationally-optimized H5 hemagglutinin influenza vaccine. *Vaccine* 37: 6022–6029. [PubMed: 31481254]
  19. Carter DM, Darby CA, Johnson SK, Carlock MA, Kirchenbaum GA, Allen JD, Vogel TU, Delagrave S, DiNapoli J, Kleanthous H, and Ross TM. 2017. Elicitation of Protective Antibodies against a Broad Panel of H1N1 Viruses in Ferrets Preimmune to Historical H1N1 Influenza Viruses. *J. Virol* 91: 1–16.
  20. Sautto GA, Kirchenbaum GA, Abreu RB, Ecker JW, Pierce SR, Kleanthous H, and Ross TM. 2020. A Computationally Optimized Broadly Reactive Antigen Subtype-Specific Influenza Vaccine Strategy Elicits Unique Potent Broadly Neutralizing Antibodies against Hemagglutinin. *J. Immunol* 204: 375–385. [PubMed: 31811019]
  21. Carter DM, Darby CA, Lefoley BC, Crevar CJ, Alefantis T, Oomen R, Anderson SF, Strugnell T, Cortés-García G, Vogel TU, Parrington M, Kleanthous H, and Ross TM. 2016. Design and Characterization of a Computationally Optimized Broadly Reactive Hemagglutinin Vaccine for H1N1 Influenza Viruses. *J. Virol* 90: 4720–4734. [PubMed: 26912624]
  22. Huang Y, França MS, Allen JD, Shi H, and Ross TM. 2021. Next Generation of Computationally Optimized Broadly Reactive HA Vaccines Elicited Cross-Reactive Immune Responses and Provided Protection against H1N1 Virus Infection. *Vaccines* 9: 793. [PubMed: 34358209]
  23. Monto AS, Malosh RE, Petrie JG, and Martin ET. 2017. The Doctrine of Original Antigenic Sin: Separating Good from Evil. *J. Infect. Dis* 215: 1782–1788. [PubMed: 28398521]
  24. Bar-Peled Y, Diaz D, Pena-Briseno A, Murray J, Huang J, Tripp RA, and Mousa JJ. 2019. A Potent Neutralizing Site III-Specific Human Antibody Neutralizes Human Metapneumovirus In Vivo. *J. Virol* 93.
  25. Huang J, Diaz D, and Mousa JJ. 2020. Antibody recognition of the pneumovirus fusion protein trimer interface. *PLoS Pathog.* 16: 1–22.
  26. Ecker JW, Kirchenbaum GA, Pierce SR, Skarlupka AL, Abreu RB, Cooper RE, Taylor-Mulneix D, Ross TM, and Sautto GA. 2020. High-Yield Expression and Purification of Recombinant Influenza Virus Proteins from Stably-Transfected Mammalian Cell Lines. *Vaccines* 8: 462.
  27. Guthmiller JJ, Dugan HL, Neu KE, Lan LY, and Wilson PC. 2019. *Human Monoclonal Antibodies*, 2nd ed. (Steinitz M, ed). Springer New York, New York, NY.
  28. Brochet X, Lefranc M-P, and Giudicelli V. 2008. IMGT/V-QUEST: the highly customized and integrated system for IG and TR standardized V-J and V-D-J sequence analysis. *Nucleic Acids Res.* 36: W503–W508. [PubMed: 18503082]
  29. O'Rourke SM, Byrne G, Tatsuno G, Wright M, Yu B, Mesa KA, Doran RC, Alexander D, and Berman PW. 2018. Robotic selection for the rapid development of stable CHO cell lines for HIV vaccine production. *PLoS One* 13: e0197656. [PubMed: 30071025]
  30. Voss NR, Yoshioka CK, Radermacher M, Potter CS, and Carragher B. 2009. DoG Picker and TiltPicker: Software tools to facilitate particle selection in single particle electron microscopy. *J. Struct. Biol* 166: 205–213. [PubMed: 19374019]
  31. Lander GC, Stagg SM, Voss NR, Cheng A, Fellmann D, Pulokas J, Yoshioka C, Irving C, Mulder A, Lau PW, Lyumkis D, Potter CS, and Carragher B. 2009. Appion: An integrated, database-driven pipeline to facilitate EM image processing. *J. Struct. Biol* 166: 95–102. [PubMed: 19263523]
  32. Suloway C, Pulokas J, Fellmann D, Cheng A, Guerra F, Quispe J, Stagg S, Potter CS, and Carragher B. 2005. Automated molecular microscopy: The new Legimon system. *J. Struct. Biol* 151: 41–60. [PubMed: 15890530]

33. Zivanov J, Nakane T, Forsberg BO, Kimanius D, Hagen WJH, Lindahl E, and Scheres SHW. 2018. New tools for automated high-resolution cryo-EM structure determination in RELION-3. *Elife* 7: 1–22.
34. Punjani A, Rubinstein JL, Fleet DJ, and Brubaker MA. 2017. cryoSPARC: algorithms for rapid unsupervised cryo-EM structure determination. *Nat. Methods* 14: 290–296. [PubMed: 28165473]
35. Pettersen EF, Goddard TD, Huang CC, Couch GS, Greenblatt DM, Meng EC, and Ferrin TE. 2004. UCSF Chimera - A visualization system for exploratory research and analysis. *J. Comput. Chem* 25: 1605–1612. [PubMed: 15264254]
36. Bangaru S, Lang S, Schotsaert M, Vandervlen HA, Zhu X, Kose N, Bombardi R, Finn JA, Kent SJ, Gilchuk P, Gilchuk I, Turner HL, García-Sastre A, Li S, Ward AB, Wilson IA, and Crowe JE. 2019. A Site of Vulnerability on the Influenza Virus Hemagglutinin Head Domain Trimer Interface. *Cell* 177: 1136–1152.e18. [PubMed: 31100268]
37. Bajic G, Maron MJ, Adachi Y, Onodera T, McCarthy KR, McGee CE, Sempowski GD, Takahashi Y, Kelsoe G, Kuraoka M, and Schmidt AG. 2019. Influenza Antigen Engineering Focuses Immune Responses to a Subdominant but Broadly Protective Viral Epitope. *Cell Host Microbe* 25: 827–835.e6. [PubMed: 31104946]
38. Boudreau CM, Yu WH, Suscovich TJ, Talbot HK, Edwards KM, and Alter G. 2020. Selective induction of antibody effector functional responses using MF59-adjuvanted vaccination. *J. Clin. Invest* 130: 662–672. [PubMed: 31845904]
39. Huang J, Diaz D, and Mousa JJ. 2020. Antibody recognition of the Pneumovirus fusion protein trimer interface. *PLOS Pathog.* 16: e1008942. [PubMed: 33035266]
40. Guthmiller JJ, Han J, Li L, Freyn AW, Liu STH, Stovicek O, Stamper CT, Dugan HL, Tepora ME, Utset HA, Bitar DJ, Hamel NJ, Changrob S, Zheng N-Y, Huang M, Krammer F, Nachbagauer R, Palese P, Ward AB, and Wilson PC. 2021. First exposure to the pandemic H1N1 virus induced broadly neutralizing antibodies targeting hemagglutinin head epitopes. *Sci. Transl. Med* 13.
41. Benton DJ, Nans A, Calder LJ, Turner J, Neu U, Lin YP, Ketelaars E, Kallewaard NL, Corti D, Lanzavecchia A, Gamblin SJ, Rosenthal PB, and Skehel JJ. 2018. Influenza hemagglutinin membrane anchor. *Proc. Natl. Acad. Sci* 115: 10112 LP – 10117. [PubMed: 30224494]
42. Guthmiller JJ, Han J, Utset HA, Li L, Lan LY-L, Henry C, Stamper CT, McMahon M, O’Dell G, Fernández-Quintero ML, Freyn AW, Amanat F, Stovicek O, Gentles L, Richey ST, de la Peña AT, Rosado V, Dugan HL, Zheng N-Y, Tepora ME, Bitar DJ, Changrob S, Strohmeier S, Huang M, García-Sastre A, Liedl KR, Bloom JD, Nachbagauer R, Palese P, Krammer F, Coughlan L, Ward AB, and Wilson PC. 2022. Broadly neutralizing antibodies target a haemagglutinin anchor epitope. *Nature* 602: 314–320. [PubMed: 34942633]

**Key Points**

Seasonally vaccinated subjects possess functional antibodies to H1 COBRA HAs.

H1 COBRA HA-reactive B cell clones were similar across vaccine seasons.

Author Manuscript

Author Manuscript

Author Manuscript

Author Manuscript

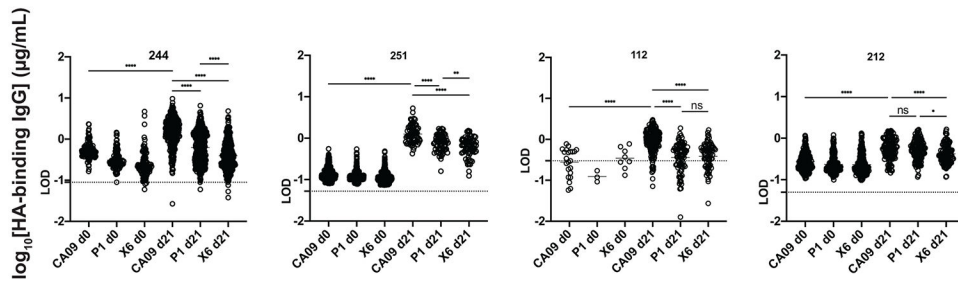


**Figure 1. Binding titers of oligoclonal B cell supernatants pre-vaccination (d0) and 21 days post-vaccination (d21) from four representative subjects.**

IgG titers against CA09 HA (CA09), P1 COBRA (P1), and X6 COBRA (X6), are shown for representative subjects receiving the 2017-2018 QIV. Supernatants from stimulated PBMCs were screened by ELISA using plates coated with the indicated antigen. PBMCs were standardized to 25,000 cells per well. Each circle indicates one well, the mean is shown as a bar, and the limit of detection (LOD) is indicated by a dotted line. LOD was calculated as three times the standard deviation of the lowest concentration divided by the slope of the standard curve for each sample, interpolated to its corresponding log concentration. Results represent one experiment. \*\*\*\* $P < 0.0001$ , \*\* $P = 0.0062$ , \* $P = 0.0216$ , ns=not significant.



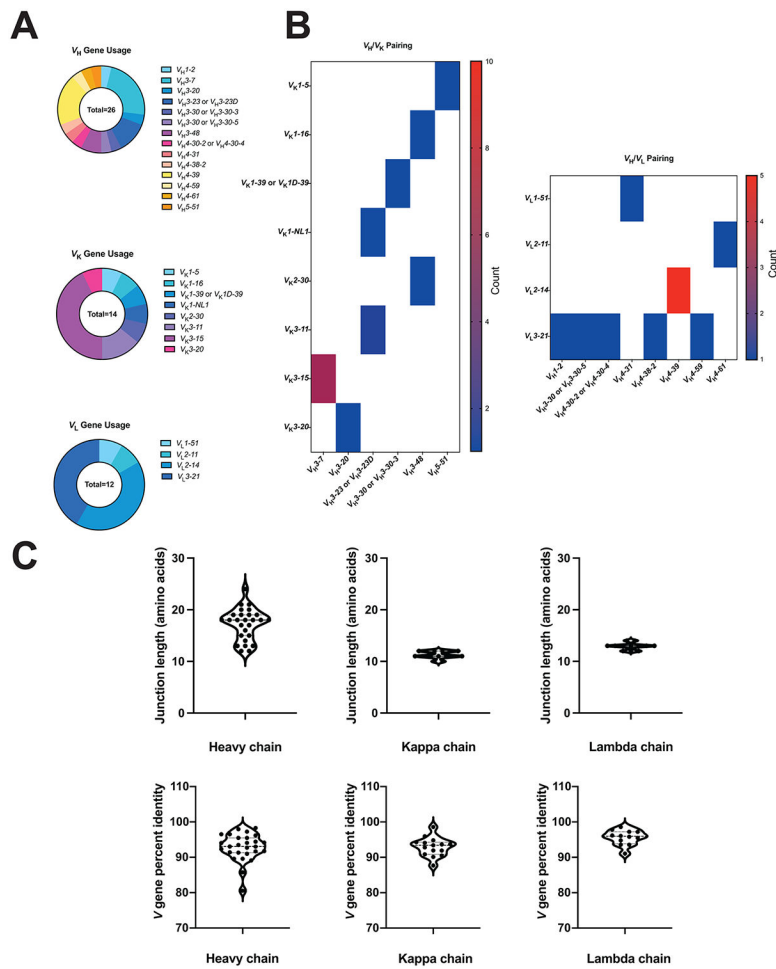


**Figure 2. Gene usage and CDR3 lengths of isolated mAbs.**

(A) The usage of heavy, kappa, and lambda chain genes are shown as a proportion of all respective genes from the panel of isolated mAbs by sequencing the hybridoma line for each clone. The pairing of heavy and light chains is shown in (B), with the number of antibodies corresponding to each pairing shown as a heat map. (C) The amino acid lengths of the heavy and light chain CDR3 regions are shown (top) alongside the nucleotide percent identity of the *V* gene to the germline sequences determined by IMGT/V-QUEST (bottom).

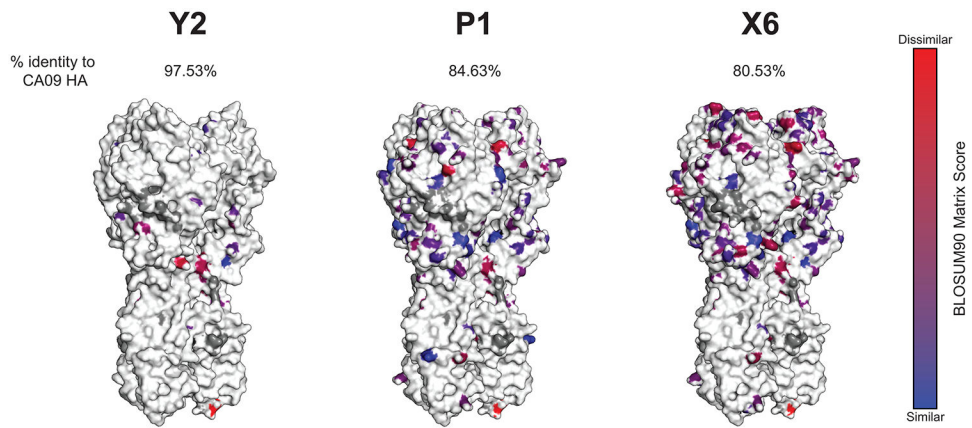


**Figure 3. Models of H1 COBRAs used in this study.**

The models of the H1 subtype COBRAs used are shown alongside the percent identity to the A/California/04/2009 HA. Substitution mutations are indicated in colors corresponding to the BLOSUM90 matrix score, a measure of the likelihood of a given amino acid mutation. White residues indicate an identical amino acid as the A/California/04/2009 HA, blue a substitution with a highly similar amino acid, and red a substitution with a highly dissimilar amino acid. Models were generated using SWISS-MODEL.

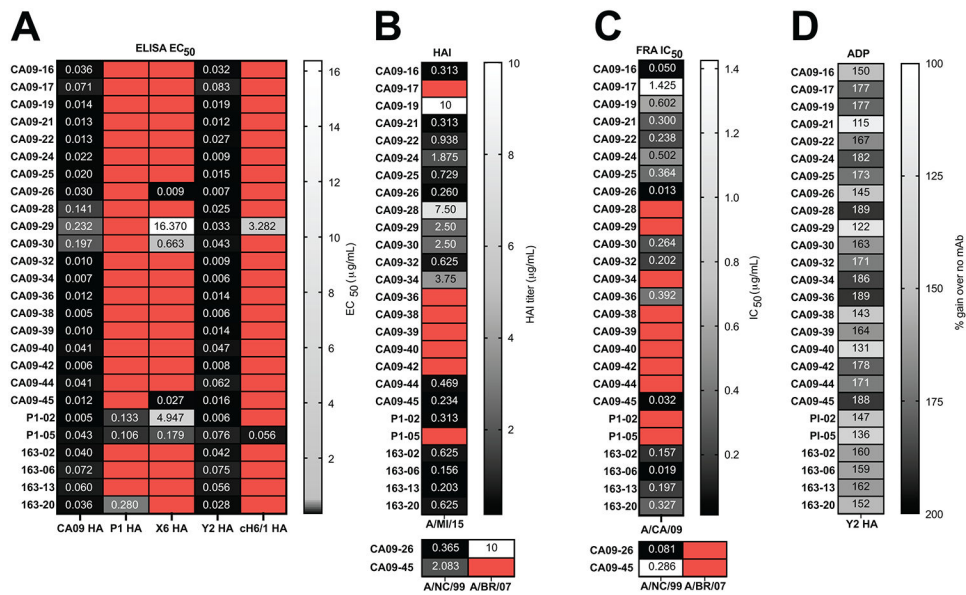


**Figure 4. Reactivity and functional activities of mAbs isolated from 2017-2018 QIV-vaccinated subjects.**

(A) Half-maximal effective concentrations (EC<sub>50</sub>s) are represented for each mAb. ELISAs were completed with each mAb serially diluted three-fold. Shown are the EC<sub>50</sub> values against CA09 HA, P1 COBRA HA, X6 COBRA HA, Y2 COBRA HA, and cH6/1 HA. For the EC<sub>50</sub> heat map, boxes in red indicate the signal at 20 μg/mL did not reach 1.5 units at 405 nm, or the calculated EC<sub>50</sub> was outside the tested concentration range due to an overall low signal. Results represent two independent experiments performed in quadruplicate. (B) HAI titers of each mAb are shown for the indicated viruses. The experiment was performed in duplicate for two independent experiments. Boxes in red indicate no HAI activity was observed at 10 μg/mL. (C) Half-maximal inhibitory concentrations (IC<sub>50</sub>s) are shown for the indicated mAbs against the viruses shown. Results represent the average of triplicate measurements for one experiment. Boxes in red indicate less than 50% neutralization at the highest concentration tested or the calculated IC<sub>50</sub> was outside the tested concentration range due to overall low neutralization activity. (D) ADP activities measured using Y2 HA-coated beads for each mAb are shown as the percentage gain over the no mAb control. Results represent one experiment performed in triplicate.

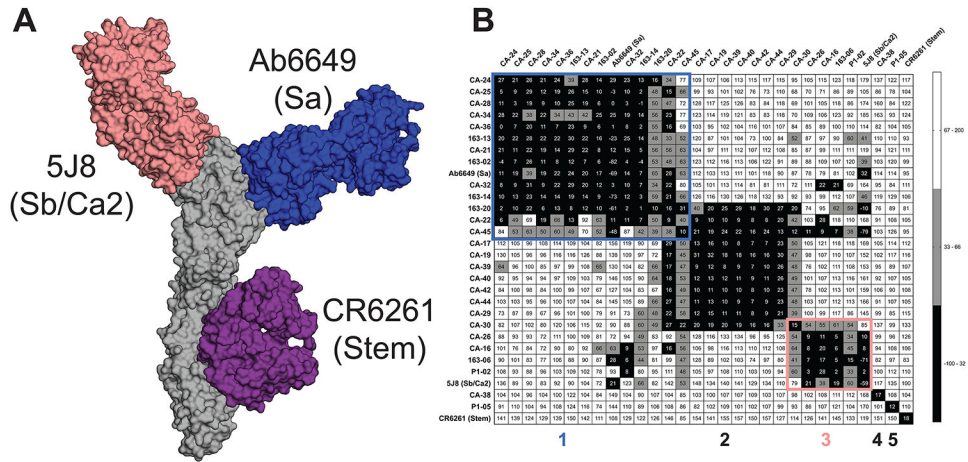


**Figure 5. Epitope binning identifies five epitopes from human antibodies isolated at 21 days post-vaccination.**  
 (A) Model of A/California/04/2009 HA in complex with Fabs of three control antibodies used for epitope binning. 5J8 and Ab6649 bind the head domain at the conserved RBS and lateral patch epitopes, respectively. CR6261 binds the stem domain at a site conserved for group 1 viruses. (B) Epitope binning was performed against A/California/04/2009 HA using full-length mAbs. Competition was measured as the percentage of the response from the association of the second antibody (horizontal axis) in the presence of the first antibody (vertical axis) as compared to the second antibody alone. Black indicates complete competition, gray moderate competition, and white no competition. Results represent one experiment with one measurement taken per competition set. Identified epitopes that have been previously characterized are outlined in blue (for the lateral patch) and pink (for the RBS). The antigenic sites of the epitopes of control mAbs Ab6649 and 5J8 are shown in parentheses.

Author Manuscript

Author Manuscript

Author Manuscript

Author Manuscript

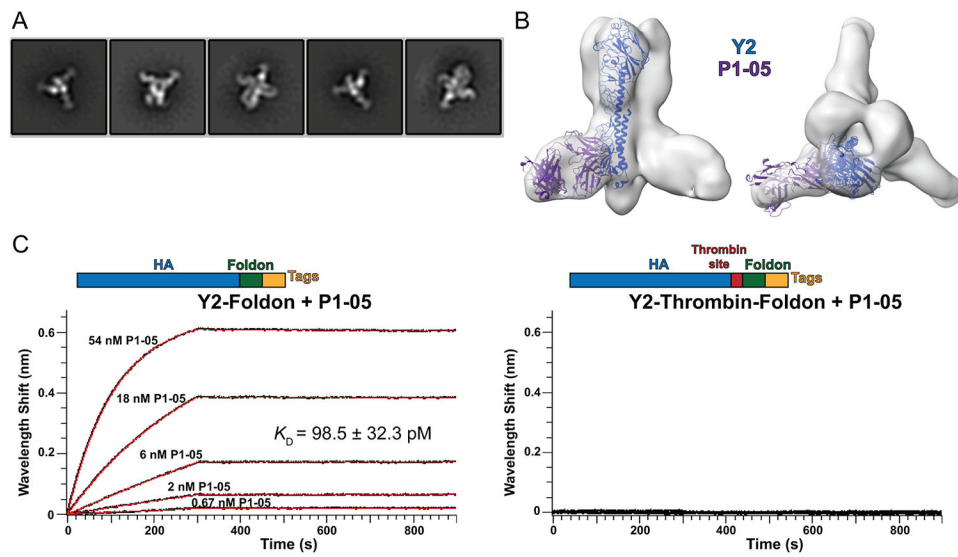


**Figure 6. Structural characterization of P1-05 binding to Y2 COBRA.**

(A) 2D class averages and (B) 3D reconstruction of the Y2+P1-05 complex. (C) Comparison of P1-05 binding with Y2 in the presence or absence of a thrombin cleavage site by biolayer interferometry. Representative runs are shown. The  $K_D$  represents the mean  $\pm$  standard deviation of three independent experiments.

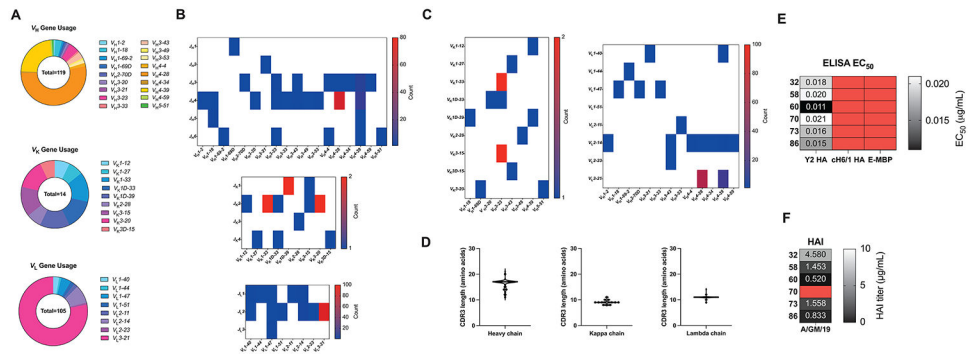


**Figure 7. Sequence characteristics of Y2 COBRA-specific B cells from a human subject receiving the 2019-2020 seasonal vaccine.**

(A) The usage of heavy, kappa, and lambda chain genes are shown as a proportion of all respective genes for all B cells with paired heavy and light chains. (B) The pairing of *V* and *J* genes are shown, with the number of B cells contributing to each pairing for each chain, as heat maps. (C) The pairing of heavy and light chain *V* genes is shown for heavy-kappa chain pairings (left) and heavy-lambda chain pairings (right) as heat maps. (D) The amino acid lengths of the CDR3 regions for the heavy and light chains are shown. (E) Six B cell receptor sequences were expressed as rAbs and tested for binding to the indicated antigens by ELISA. E-MBP, negative control. The experiment was performed twice, and measurements taken in quadruplicate. (F) HAI activity of these six rAbs against A/Guangdong-Maonan/SWL-1536/2019. Results represent the average of two independent experiments with measurements taken in duplicate. Red indicates no activity for either assay in (E) and (F).